Multifractal analysis of the atomic spectral line series

Andrés Sáiz* and Vicent J. Martínez†
Departament d'Astronomia i Astrofísica, Universitat de València, Burjassot, 46100 València, Spain
(Received 29 November 1995; revised manuscript received 9 May 1996)

We have used the multifractal approach for the characterization of the spectral line series of energized atoms. We show how the wavelength distribution of lines follows the characteristic scaling of the multifractal sets. This technique provides us with a way of describing the properties of the clustering of lines in the spectra. We have used a multiplicative multifractal model to test the reliability of the method when applied to the usual number of lines of experimentally obtained spectra. By means of the multiscaling approach we can control the robustness of the method when applied to sets of lines censored below a given density threshold. [S1063-651X(96)03109-1]

PACS number(s): 05.45.+b, 32.30.−r, 64.60.Ak

I. INTRODUCTION

The spectral line series associated to an energized atom is the sequence of wavelengths characterizing its electromagnetic radiation. Each element has its own characteristic series of spectral lines. Hydrogen displays the well known five series in different parts of the spectrum: the Balmer series in the visible region, the Lyman lines in the ultraviolet, and the Paschen, Brackett, and Pfund series lying in the infrared. The wavelength distribution of the lines expressed in terms of the inverse wavelength is remarkably well represented by Balmer's formula

$$\frac{1}{\lambda}=R\left(\frac{1}{m^2}-\frac{1}{n^2}\right), \quad n>m, \tag{1.1}$$

with $m=2$ for the Balmer series, and $m=1,3,4,5$ for Lyman, Paschen, Brackett, and Pfund series, respectively. R denotes the Rydberg constant.

Similar formulas exist for the atoms of the alkali metals and other hydrogenlike elements like singly-ionized helium. Experimental spectral line series corresponding to other atoms are also available. The spectrum of atoms like iron or cobalt are visually more complicated than the spectrum of the hydrogen atom and obviously they do not appear to show the same regularity in spacing. Nevertheless, the distribution of the spectral lines of these atoms might be an interwoven superposition of formulas similar to Balmer's.

In this paper we will see that the wavelength distribution of the emission lines of the spectrum of energized atoms follows some kind of multifractal scaling.

II. THE MULTIFRACTAL SCALING

In order to study, by means of the multifractal analysis [1], the spectral line series within a segment of wavelengths, we will normalize the length of the segment to unity. Performing a partition of the unit segment into cells of size r, we count the number of lines lying within each one, $n_i(r)$. Multifractal scaling holds if

$$Z(q,r)=\sum_{i=1}^{N(r)}\left(\frac{n_i(r)}{N}\right)^q \propto r^{\tau(q)}, \tag{2.1}$$

N being the total number of lines. The quantities defined as $D(q)=\tau(q)/(q-1)$ are known as Rényi dimensions or generalized dimensions [2,3]. This function characterizes the scaling properties of the multifractal set.

An alternative description is provided by the $f(\alpha)$ function [4,5]. If the cell-counts can be expressed as a power law of the scale, $p_i(r)=(n_i(r)/N)=r^{\alpha_i}$. Multifractal scaling implies that the distribution of the α values (also known as Hölder exponents) is

$$n(\alpha)d\alpha \sim |\ln r|^{1/2} r^{-f(\alpha)} d\alpha, \tag{2.2}$$

where $n(\alpha)d\alpha$ is the number of times α takes a value in a given interval $[\alpha,\alpha+d\alpha]$ [3]. The distribution of the Hölder exponents α is related with $\tau(q)$ through a Legendre transformation [4,6].

A. An illustrative multifractal model

To illustrate the multifractal behavior in a controllable set of lines similar to the spectral line series, we will consider a multiplicative multinomial cascade in the unit interval, used extensively to mimic turbulent processes [5,7,8]. Dividing the unit interval into s pieces, we assign a probability $p_1,p_2\ldots,p_s$ to each of the subintervals $(p_1+p_2+\cdots+p_s=1)$. Each subinterval is then subdivided into s pieces in the same way as the parent, and we assign to each of the subdivisions one of the numbers p_i. The value attached to a new subdivision is the product of this p_i value with its parent and all its ancestors. We continue the cascade until L levels have been constructed, leaving at the end s^L subintervals with a measure $\{p_{i1}p_{i2}\cdots p_{iL}\}_{i=1}^{s^L}$, $(p_{ij}\in\{p_1,p_2,\ldots,p_s\})$ attached to each one. If n $(n\leqslant s)$ is the number of nonzero p_i values, it is straightforward to see that in the limit when $L\to\infty$,

*Electronic address: andressa@evalvx.ific.uv.es
†Electronic address: martinez@hubble.matapl.uv.es

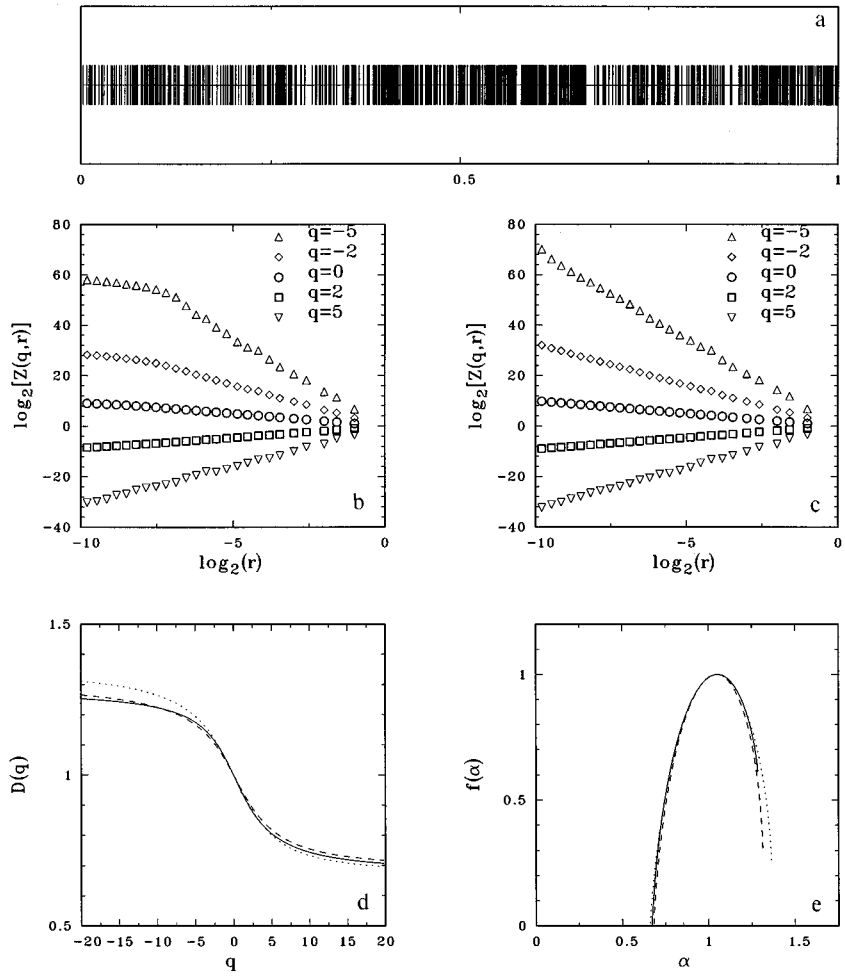

FIG. 1. (a) A realization of the multiplicative multinomial cascade. 1012 lines are shown in the model. (b) The partition sum $Z(q,r)$ for different values of q, calculated for the set of lines shown in (a). (c) The same function as in (b) but for the set with $N=10\,000$ lines. (d) The function $D(q)$ for the sets with $N=1012$ (dotted line) and $N=10\,000$ (dashed line). A solid line stands for the theoretical prediction. (e) The $f(\alpha)$ function [different line styles represent the same as (d)].

$$D(q)=(1-q)^{-1}\frac{\ln(\Sigma_{i=1}^{n}p_i^q)}{\ln s} \tag{2.3}$$

and the $f(\alpha)$ spectrum is given by

$$\alpha(q)=\frac{\Sigma_{i=1}^{n}p_i^q \ln p_i}{\ln(1/s)\Sigma_{i=1}^{n}p_i^q} \tag{2.4}$$

and

$$f(\alpha(q))=\frac{q\Sigma_{i=1}^{n}p_i^q\ln p_i-(\Sigma_{i=1}^{n}p_i^q)(\ln\Sigma_{i=1}^{n}p_i^q)}{\ln(1/s)\Sigma_{i=1}^{n}p_i^q}. \tag{2.5}$$

In Fig. 1(a) we show a realization of a multiplicative multinomial cascade with $s=6$ and number of levels $L=4$. First we have distributed 10 000 lines into the s^L subintervals accordingly to the probabilities assigned to each of the s^L subintervals. Only 1012 randomly selected lines have been plotted in the figure. The values of the initial probabilities used in this example are $p_1=0.1$, $p_2=0.1$, $p_3=0.1$, $p_4=0.2$, $p_5=0.2$, $p_6=0.3$.

Equations (2.3)–(2.5) are the analytical expressions for the Rényi dimensions and the $f(\alpha)$ curve, respectively. Nevertheless, we want to test how the scaling relation (2.1), used for practical purposes, works for a limited number of lines. As we will show, we are able to get reliable results for the multifractal curve $D(q)$ using Eq. (2.1) when applied to this multifractal set having only $\sim 10^3$ lines.

We have considered two realizations: one with 1012 lines [Fig. 1(a)] and a second one with 10 000 lines. As we have already said, the first one has been extracted randomly from the second one. Figure 1(b) show the log-log plots of different q-moments vs the scale r for the set with 1012 lines. Figure 1(c) is the same but for the set with 10 000 lines. In both cases the fitted slope provides the estimation of $\tau(q)$. The scaling range where the power law of Eq. (2.1) holds is 2^{-8} to 2^{-1} for the set with $N=1012$ lines and it is broader for the set with $N=10\,000$ lines as we can easily see in the figures. In the first case, the number of occupied cells does not increase when the scale r gets values below a given one. This discreteness effect breaks the scaling at small scales.

The corresponding $D(q)$ and $f(\alpha)$ curves are plotted in Figs. 1(d) and 1(e) with dotted lines for $N=1012$ and dashed lines for $N=10\,000$, respectively. The solid lines show the expected theoretical functions displayed in Eqs. (2.3)–(2.5). The agreement is rather good even for the set with fewer lines.

III. MULTIFRACTALS IN THE ANALYSIS OF REAL SPECTRA

The previous simulated spectra were by construction multifractal sets. We are going to study now the part of the

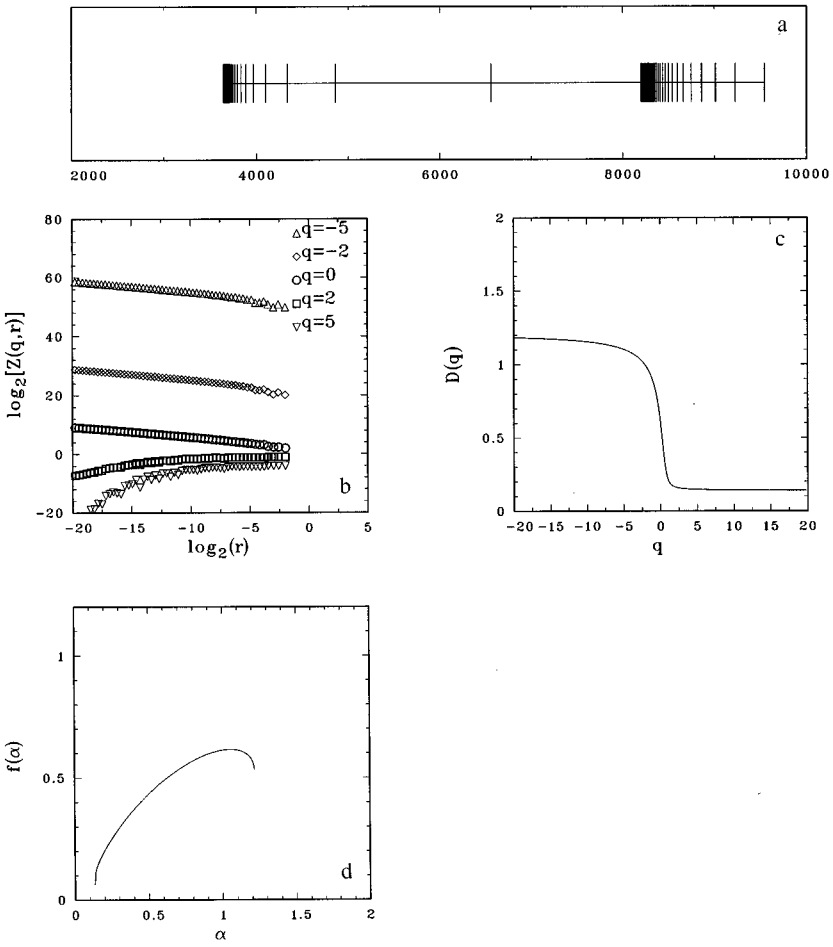

FIG. 2. (a) The Balmer and Paschen series of the hydrogen atom. (b) The function $Z(q,r)$ for different values of q calculated for the set of lines shown in (a). (c) The $D(q)$ function for this spectral line series. (d) The corresponding $f(\alpha)$ spectrum.

spectra with wavelength in the range 2000−10 000 angstroms for three nonionized atoms: hydrogen, argon, and cobalt. In the first case we use the Balmer and Paschen series represented in Fig. 2(a), while for the other two cases we use the data in the table of wavelengths published by MIT [9] [see Figs. 3(a) and 4(a)]. As a first approximation intensities and widths of the lines are not considered. We are just interested in their distribution along the wavelength segment. The number of lines used in each case is $N=996$ for hydrogen, $N=611$ for argon, and $N=1455$ for cobalt. In Figs. 2(b), 3(b), and 4(b) we show the log-log plots of the partition function $Z(q,r)$ versus r corresponding to the spectral line series of the three atoms. In each case five different values of q have been selected. The scaling range where a power law holds is 2^{-6} to 2^{-1} for the spectra corresponding to argon and cobalt and 2^{-10} to 2^{-1} for the series of the hydrogen atom. After fitting a power law within these ranges we have obtained the exponents $\tau(q)$ following Eq. (2.1). The corresponding $D(q)=\tau(q)/(q-1)$ functions are plotted in Figs. 2(c), 3(c), and 4(c). By doing a numerical Legendre transformation we have obtained the $f(\alpha)$ curves shown in Figs. 2(d), 3(d), and 4(d). This analysis allows us to conclude that the multifractal spectrum might be used to characterize the inherent scaling properties of the wavelength distribution of the spectral line series. We can see that for the hydrogen spectrum the capacity dimension is $D(0)\simeq 0.61$ much less than 1, while argon and cobalt present values of $D(0)\simeq 0.96$ and $D(0)\simeq 1.00$, respectively. In 1D, when $D(0)=1$ the distribution is known as a fat fractal. The value of $D(0)\simeq 1$ is due to the fact that the spectral line series of argon and cobalt are more space filling than the Balmer series, but still they display multifractal properties. The capacity dimension of the part of the hydrogen spectrum analyzed numerically in this paper is rather similar to the fractal dimension of the ternary Cantor set $D(0)=\log 2/\log 3\simeq 0.63$. For a similar discrete example, it is worth mentioning that the set of points defined by $\{1/n\}_{n=1}^{\infty}$ has capacity dimension $D(0)=1/2$.

The value of $\alpha_{\min}$ [or equivalently $D(+\infty)$] is $\simeq 0.14$ for the hydrogen atom and $\simeq 0.6$ for argon and cobalt. Since this exponent is the one corresponding to the regions with highest density of the spectral line series, the previous difference has to be interpreted in terms of the scaling $p_i(r)=r^{\alpha_i}$. The number of lines in the vicinity of the denser regions grows more rapidly for the selected lines of the Balmer and Paschen series than for all the experimental spectral lines of argon and cobalt.

For $q\geqslant 0$ the $D(q)$ functions for argon and cobalt are rather similar, showing that the high density regions of the spectral lines of both elements are rather similarly distributed. This similarity can be appreciated also in the left branch of corresponding $f(\alpha)$ curves. The differences between the line series of these atoms appear for $q<0$ corresponding to the low density zones of the spectral line series [see also the right branch of the $f(\alpha)$ curve]. The value of

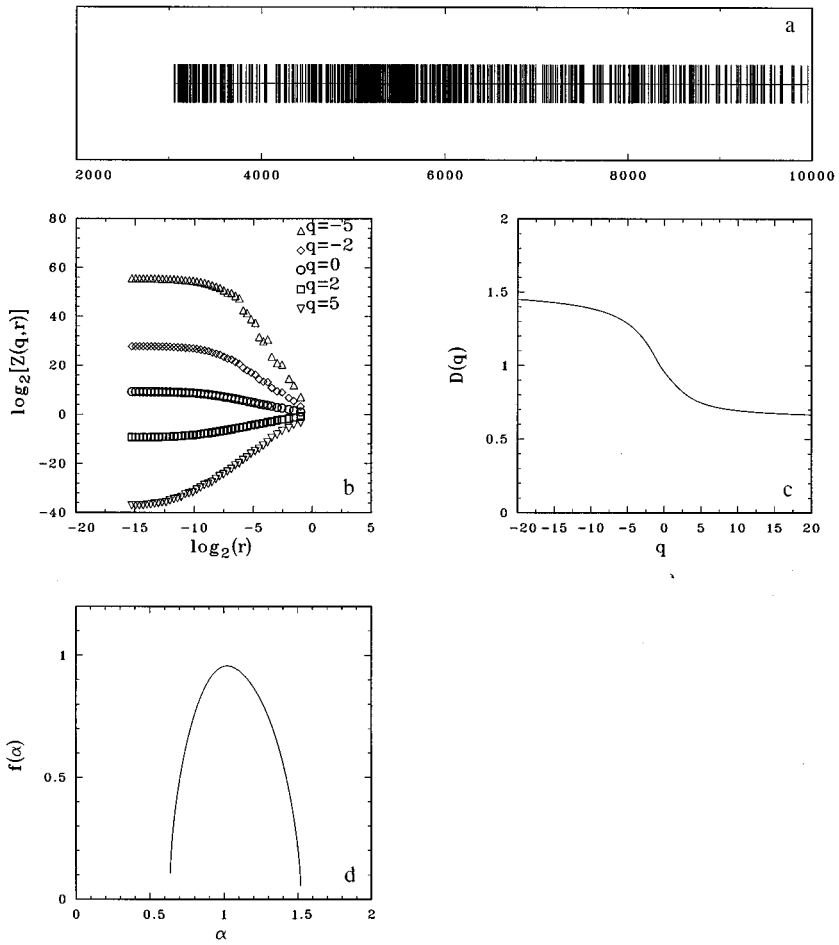

FIG. 3. The same as Fig. 2 but for argon.

$\alpha_{\max}$ [or equivalently $D(-\infty)$] is larger for cobalt, $\alpha_{\max}\simeq 1.75$, than for argon, $\alpha_{\max}\simeq 1.52$, and both are larger than the value corresponding to the spectral series of the hydrogen atom, $\alpha_{\max}\simeq 1.22$. This fact shows how the scaling index corresponding to the low density regions changes from one set of lines to another. The difference $\alpha_{\max}-\alpha_{\min}$ is larger for cobalt than for argon. This is an interesting feature which reveals that the distribution of the lines in the wavelength interval is more inhomogeneous for the spectrum of cobalt than for the spectrum of argon. It is also interesting to note that for the Balmer series of the hydrogen atom $f(\alpha_{\max})\simeq 1\neq 0$ and therefore the rightmost part of the $f(\alpha)$ curve resembles a hook. In the other two cases $f(\alpha_{\max})\simeq 0$. This fact implies that the dimensionality of the most rarefied part of the spectra for argon and cobalt is zero, corresponding to a single point, while it is $\simeq 1$ for hydrogen, corresponding to a set of points with finite nontrivial dimension.

IV. MULTISCALING

It should be possible that some spectral lines were not seen because of experimental poor resolution or because they are extremely weak compared with other lines (e.g., the well known forbidden lines in astronomical spectroscopy detected in the spectra of certain H II regions). We can model this possible lack of information by means of the multiplicative multifractal cascade in which all last generation cells with an attached probability below a certain threshold ϵ are just assigned with zero probability. In other words, if the density of lines within such a cell is less than ϵ, we consider that this cell is indistinguishable from a real zero density cell. We are now interested in how the functions $D(q)$ and $f(\alpha)$ look for the censored set. We will see that the characteristic exponents are slowly varying functions of the threshold density. This phenomenon is known as multiscaling [10–12]. Although it is known that multifractality implies multiscaling, multiscaling could be a more general phenomenon [13].

In Fig. 5, we see the model shown in Fig. 1(a) after applying two different density thresholds $\epsilon_1=8\times 10^{-4}$ and $\epsilon_2=1.6\times 10^{-3}$. In the first case 719 lines have survived after thresholding, while only 413 have remained in the second case. In Fig. 6(a) we show the partition sum $Z(2,r)$ as a function of r in a log-log plot. The function corresponding to the whole set without any threshold is displayed with a dotted line. The solid line corresponds to the expected analytical solution. It is remarkable how good the agreement is between these two lines. The long-dashed line corresponds to the set after applying the first threshold ϵ_1, while the short-dashed line comes from the second density threshold ϵ_2. Although the expected multiscaling deviations appear clearly noticed in the plot, the differences between the slopes are smaller than in Fig. 6(b), where we show the function $Z(-5,r)$ for the same sets. As we can see, differences are much pronounced for the moment $q=-5$ than for $q=2$. This is due to the fact that negative moments emphasize the low density regions of the multifractal set. For negative q,

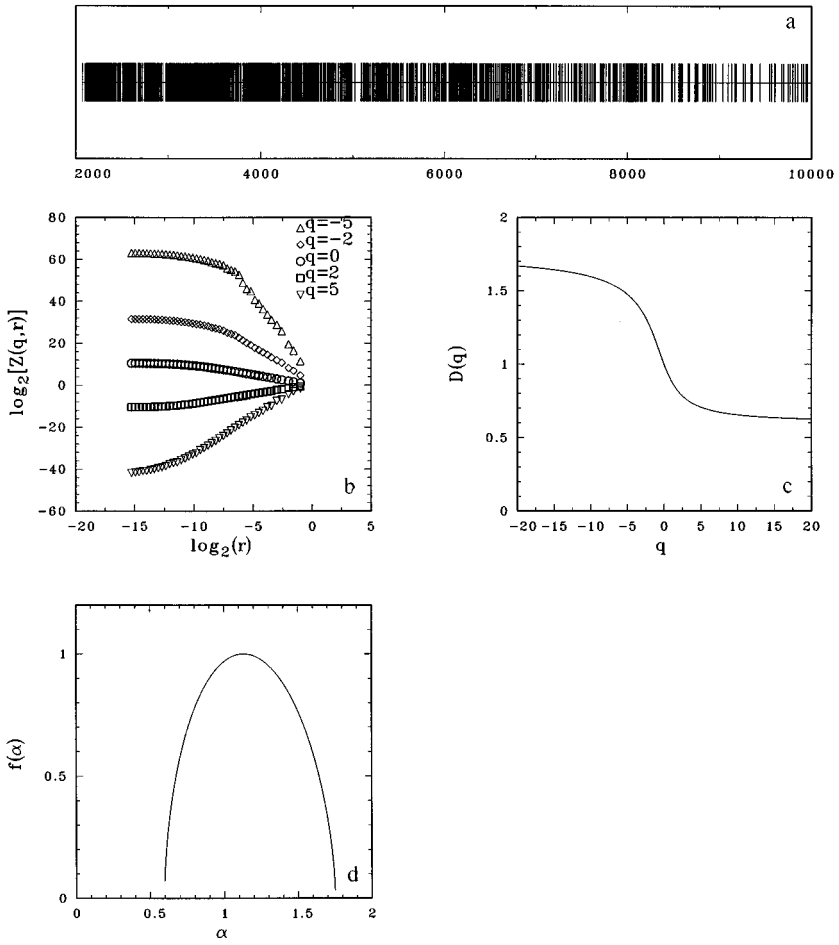

FIG. 4. The same as Fig. 2 but for cobalt.

scaling ranges vary with the density threshold. Moreover, the slope of these curves within the scaling range, $\tau(q)$, changes with the density cutoff as is usual in the multiscaling approach. The function $Z(q,r)$ of the censored sets tends asymptotically to the function corresponding to the uncensored set for large values of r. This tendency is more evident for $q=2$ than for $q=-5$. The denser regions are less affected by thresholding, and obviously the moments corresponding to positive values of q are less changed. These trends are appreciated globally in Figs. 6(c) and 6(d). In these plots we show the functions $D(q)$ and $f(\alpha)$ corresponding to the whole set (dotted line) and to the set after applying the density threshold ϵ_1 (dashed line). The solid lines correspond to the theoretical predictions of Eqs. (2.3)–(2.5) when no density cutoff is applied and to their corresponding counterparts when a density threshold is used to censor the set. The function $\tau(q)$ is obtained as the slope of the log-log plot of $Z(q,r)$ vs r. The fit is performed within the scaling range where the power law holds. This range obviously depends on the density threshold as can be easily appreciated in Figs.

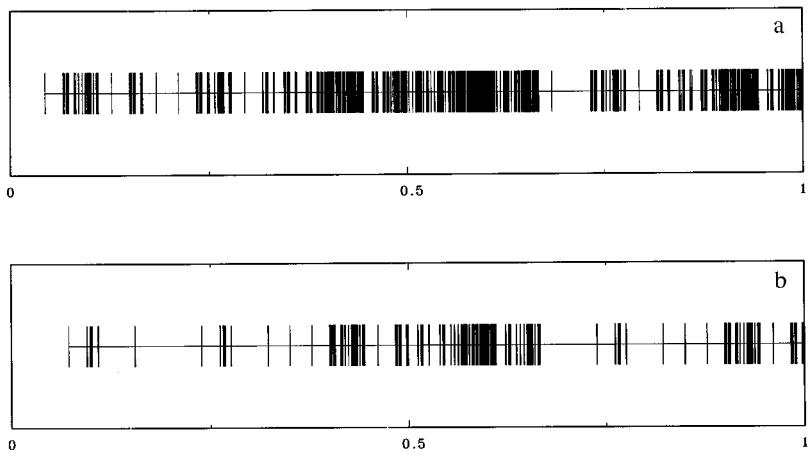

FIG. 5. Censored realizations of the multiplicative multifractal cascade after applying a density threshold: (a) $\epsilon_1=8\times10^{-4}$ and (b) $\epsilon_2=1.6\times10^{-3}$.

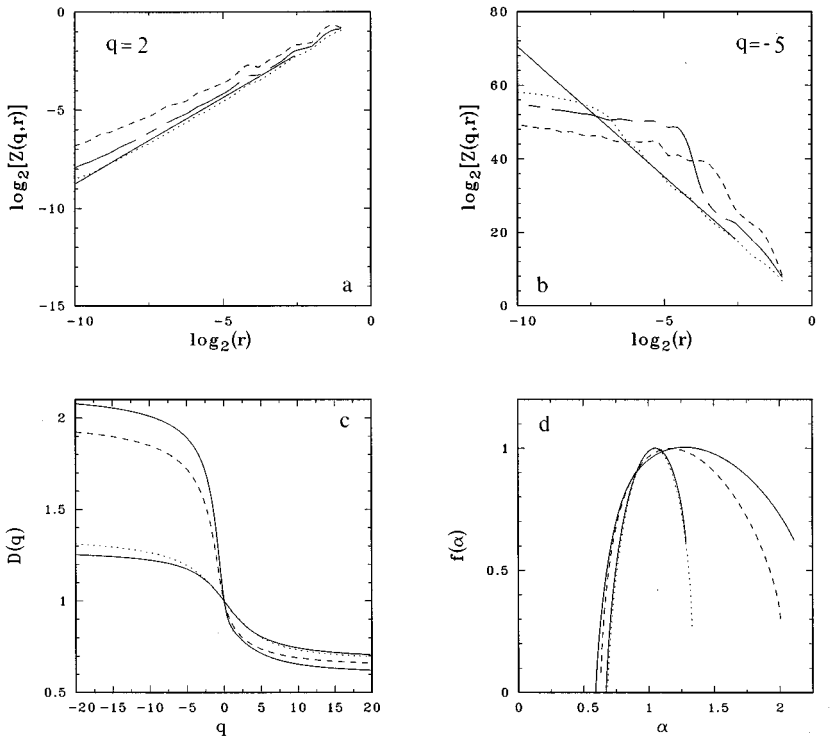

FIG. 6. (a) The partition sum $Z(2,r)$ for the multiplicative cascade: the solid line corresponds to the theoretical prediction, the dotted line to the realization with $N=1012$ lines without any cutoff, the long-dashed line corresponds to the first density threshold ϵ_1, and the short-dashed line to ϵ_2. (b) The same as (a) but for $q=-5$. (c) The function $D(q)$ for the whole set with $N=1012$ lines (dotted line). The theoretical result of Eq. (2.8) is the solid line lying close to the dotted one. The dashed line corresponds to the density threshold ϵ_1, and again the solid line close to this one is the theoretical prediction for this case. (d) The same as (c) but for the $f(\alpha)$ curve.

6(a) and 6(b). It is interesting to notice that the value of the capacity dimension $D(0)$ is not appreciably affected by the density threshold. The multiscaling deviations appear more clearly noticeable for $D(q)$ when $q<0$; consequently the right-hand branch of the $f(\alpha)$ spectrum is more strongly affected by the density cutoff. This is due to the fact that the size of the empty regions increases when we remove lines belonging to subintervals with probability less than the given threshold.

We have also performed the multiscaling analysis of the experimental line series of cobalt. As we can see in Fig. 7, the behavior previously found for the multiplicative model is well reproduced by the real data. We have applied two density thresholds in order to remove 13% and 20% of the lines,

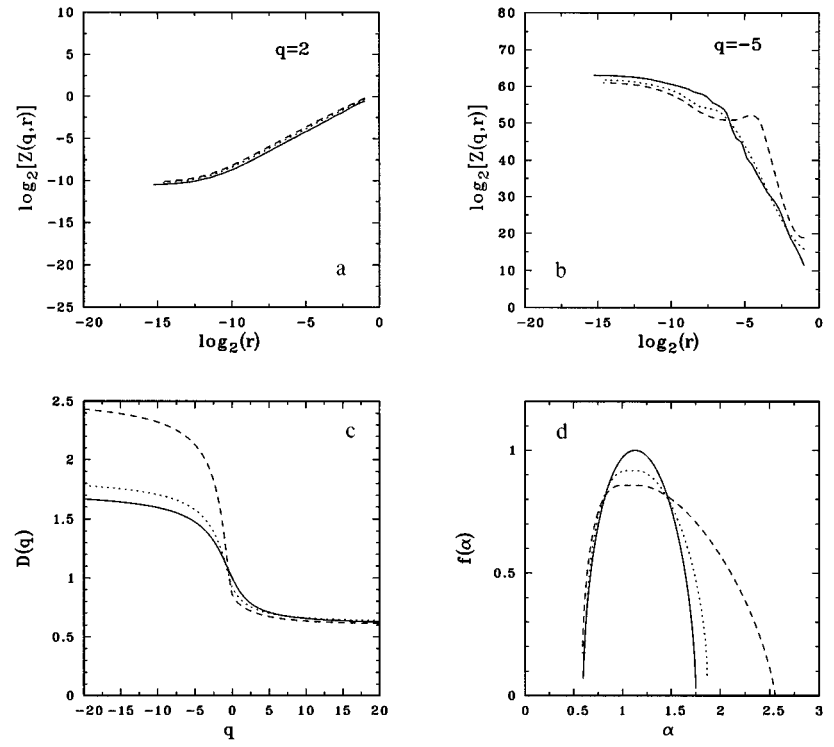

FIG. 7. The same as Fig. 6 but for the experimental line series of cobalt. In all panels, the solid line corresponds to the whole data set, while the dotted and dashed lines correspond to removing 13% and 20%, respectively, of the spectral lines in the low density regions.

respectively. The removed lines obviously lie in the low density regions of the wavelength distribution. In Fig. 7(a), we can appreciate that the slope of the log-log plot of $Z(2,r)$ vs r is nearly not affected by the density cutoff, while for $Z(-5,r)$ the threshold affects both the scaling range and the slope [see Fig. 7(b)]. The corresponding $D(q)$ and $f(\alpha)$ functions are shown in Figs. 7(c) and 7(d). The same trends already seen with the multiplicative model are observed in the analysis of the real data.

V. CONCLUSION

We have introduced the multifractal techniques to analyze the spectral line series associated to energized atoms. The distribution of the lines along a segment of wavelengths seems to show clear scaling properties in a given range of wavelengths. We have tested the method in a simple model to generate artificial multifractal spectra in 1D by means of a multiplicative cascade. The model has the virtue of possessing an analytical expression for the multifractal curves $D(q)$ and $f(\alpha)$. We have shown that a number of lines of the order of 1000 is enough to obtain rather good estimates of these multifractal functions by means of the box-counting algorithm.

We have analyzed the spectral line series of several atoms (hydrogen, cobalt, and argon). The main characteristics of the wavelength distribution of lines are clearly interpretable looking to their corresponding $D(q)$ or $f(\alpha)$ curves. The simpler structure of the hydrogen spectrum is clearly noticed in the nearly bifractal behavior of its $D(q)$ function. A bifractal is qualitatively similar to the power-law singularity measure of Ref. [4].

By means of the multifractal quantities, we can compare quantitatively the spectral line series of different atoms. Therefore, this approach provides us with a kind of characterization of the spectral line series.

The reliability of the multifractal description is tested against possible experimental missed lines. The test is performed by means of the multiscaling approach. In this approach, regions of the multifractal set with local density below a given threshold ϵ are erased. The corresponding multifractal exponents $\tau(q)$ are slightly varying functions of the density threshold. For the multiplicative model used here, the deviations from the original multifractal functions are much more significant for negative values of q. Since denser regions are obviously less affected, the function $D(q)$ for $q>0$ [or equivalently the left-hand branch of $f(\alpha)$] remains more stable after censoring the set with the density cutoff.

It seems reasonable that some kind of order exists in the distribution of the energy states of an atom and as a consequence in its emission spectrum. In Ref. [14], Kohmoto *et al.* have analyzed the scaling of the self-similar wave functions of the energy spectrum of one-dimensional quasicrystal models. Our work seems to imply that, within a certain range, the wave function of an atom should be self-similar as a consequence of the observed multifractal self-similarity of its line spectrum.

ACKNOWLEDGMENTS

This research is partially supported by the project No. GV-2207/94 of the Conselleria d'Educació i Ciència de la Generalitat Valenciana. We are grateful to E. Saar and B. Jones for valuable comments.

[1] G. Paladin and A. Vulpiani, Phys. Rep. **156**, 147 (1987).
[2] P. Grassberger and I. Procaccia, Physica D **13**, 34 (1984).
[3] P. Grassberger, R. Badii, and A. Politi, J. Stat. Phys. **51**, 135 (1988).
[4] T.C. Halsey, M.H. Jensen, L.P. Kadanoff, I. Procaccia, and B.I. Shraiman, Phys. Rev. A **33**, 1141 (1986).
[5] R. Benzi, G. Paladin, G. Parisi, and A. Vulpiani, J. Phys. A **17**, 3521 (1984).
[6] V.J. Martínez, B.J.T. Jones, R. Domínguez-Tenreiro, and R. van de Weygaert, Appl. J. **357**, 50 (1990).
[7] C. Meneveau and K.R. Sreenivasan, Phys. Rev. Lett. **59**, 1424 (1987).
[8] M. Nelkin, J. Stat. Phys. **54**, 1 (1989).
[9] *Tables of Wavelengths* (MIT Press, Cambridge, 1969).
[10] M.H. Jensen, G. Paladin, and A. Vulpiani, Phys. Rev. Lett. **67**, 208 (1991).
[11] G. Paladin, M. Vergassola, and A. Vulpiani, Physica A **185**, 174 (1992).
[12] V.J. Martínez, S. Paredes, S. Borgani, and P. Coles, Science **269**, 1245 (1995).
[13] A. Coniglio and M. Zanneti, Physica D **38**, 37 (1989).
[14] M. Kohmoto, B. Sutherland, and C. Tang, Phys. Rev. B **35**, 1020 (1987).